



# Two step method for preparing TiO<sub>2</sub>/Ag/rGO heterogeneous nanocomposites and its photocatalytic activity under visible light irradiation

Tian Tang<sup>1</sup> · Tao Wang<sup>1,2</sup> · Yang Gao<sup>1</sup> · Huan Xiao<sup>1</sup> · JiaHui Xu<sup>1</sup>

Received: 26 October 2018 / Accepted: 18 March 2019 / Published online: 28 March 2019  
© Springer Science+Business Media, LLC, part of Springer Nature 2019

## Abstract

Because the Fermi level of precious metal silver and titanium dioxide are different, the contact between the two can form a Schottky barrier, which is beneficial to reduce the recombination rate of photogenerated electron pairs. The unique surface plasmon resonance effect of the silver can promote the absorption of light by titanium dioxide, thereby increasing the utilization of light by the composite. Graphene not only has excellent electrical conductivity, but also has a large specific surface area and good adsorption capacity, and is considered to be the most potential carrier. In this study, we introduced silver and graphene into TiO<sub>2</sub> nanowires, and prepared TiO<sub>2</sub>/Ag/rGO heterogeneous nanocomposites. Firstly, the morphology of titanium dioxide was modified by high-voltage electrospinning technology to increase its specific surface area and increase its active site involved in photocatalysis. Then, using hydrothermal method combines the good characteristics of reduced graphene oxide (rGO) and precious metal silver, enhances the transfer of photogenerated electrons, and prolongs the lifetime of photogenerated electron–hole pairs. Thereby, the photocatalytic activity of the composite material is improved, so the prepared TiO<sub>2</sub>/Ag/rGO heterogeneous nanocomposites can degrade the rhodamine B solution by 92.9% in 80 min.

## 1 Introduction

With the rapid development of the degree of industrialization in the world, the continuous improvement of people's living standards, and the huge demand and consumption of fossil fuels, the industrial pollution problem has become increasingly serious and has caused widespread concern. Therefore, the problem of environmental pollution has become a new challenge for mankind. The current main methods for improving environmental pollution include, in principle, biological, physical and chemical methods. The ultimate goal of these three methods is to convert organic pollutants in solution into small molecules that are environmentally

friendly, such as titanium dioxide and water. Compared with traditional degradation technology, photocatalytic degradation of organic pollutants has the advantages of low energy consumption and high efficiency, which is considered to be the most industrially feasible way [1–4]. Among many photocatalytic materials, TiO<sub>2</sub> is considered to be the most promising semiconductor material because of its low price, nontoxicity, good stability and no secondary pollution [5–7]. However, there are several drawbacks; for instance, the low light absorption region and low quantum yield which hinder TiO<sub>2</sub> further application. Noble metal is introduced into TiO<sub>2</sub> to enhance photocatalytic activity in the visible region is gradually concerned and considered to be a good solution to overcome this problem, for example, silver modified titanium dioxide [8, 9]. In addition, when Ag nanoparticles are distributed on the surface of TiO<sub>2</sub>, after irradiated with ultraviolet light, silver nanoparticles can capture electrons in the conduction band of TiO<sub>2</sub>, thereby preventing electron–hole recombination [10–13].

Since graphene was discovered by scientists Geim and Novoselov of the University of Manchester, it has attracted great attention. As the unbonded  $\pi$  electrons in graphene can move freely over the entire plane, it has carriers with

✉ Tao Wang  
wangt0428@163.com

<sup>1</sup> Key Laboratory of Atomic and Molecular Physics & Functional Materials of Gansu province, College of Physics and Electronic Engineering, Northwest Normal University, Lanzhou 730070, People's Republic of China

<sup>2</sup> College of Physics and Electronic Engineering, Northwest Normal University, Lanzhou 730070, Gansu, People's Republic of China

extremely high migration rates, and the temperature does not have much influence on the electron migration rate in graphene. Moreover, graphene is a two dimensional planar material composed of a single layer of carbon atoms, which has high transparency and can absorb part of visible light [14]. So it can be used as an excellent carrier for a photocatalyst. In addition, the high conductivity of graphene can increase the electron transfer rate of the TiO<sub>2</sub> conduction band, thereby prolonging the lifetime of electron–hole pairs and improving the photocatalytic activity of the nanocomposite [15–17].

In this paper, TiO<sub>2</sub>/Ag/rGO heterogeneous nanocomposites were synthesized through electrospinning combined with hydrothermal reaction. First, TiO<sub>2</sub>/Ag nanowire was prepared by an electrospinning technique, and then TiO<sub>2</sub>/Ag/rGO nanocomposite was prepared using a hydrothermal kettle in a mixed solution of H<sub>2</sub>O and ethanol. Ethanol acts as a solvent and reagent in the high temperature and high pressure hydrothermal process to reduce graphite oxide (GO) to reduced graphene oxide (rGO). The strong interaction between TiO<sub>2</sub> nanowires and silver nanoparticles promotes the transfer of electrons. rGO increases the specific surface area of the composite and provides more active sites for photocatalyst degradation of contaminants. Thereby improving the photocatalytic activity of the TiO<sub>2</sub>/Ag/rGO heterogeneous nanocomposites.

## 2 Experimental section

All chemical materials used are analytical grade and the water used is deionized water.

The GO was prepared by the method of Hummer's and improved [18]. The preparation of TiO<sub>2</sub> nanowires referenced to previous work of our research group [7, 17]. The TiO<sub>2</sub>/Ag/rGO nanocomposites was synthesized by hydrothermal method. First, a certain quantity of GO was added into deionized water. Next, TiO<sub>2</sub>/Ag nanowires and ethanol were added into GO solution and underwent sonication. Then, the solution was transferred to teflon-lined autoclave, and 150 °C for 12 h. After the teflon-lined autoclave was naturally cooled to room temperature, the supernatant was decanted, and the resulting gray precipitate was dissolved in absolute ethanol and deionized water, washed by centrifugation, and dried at 60 °C for 10 h.

## 3 Results and discussions

### 3.1 XRD analysis

The phase characteristics of samples were characterized by X-ray diffraction. The XRD pattern of TiO<sub>2</sub> and TiO<sub>2</sub>/Ag/

rGO nanocomposites were showed in Fig. 1. Figure 1 shows the TiO<sub>2</sub> nanocomposites appeared several diffraction peaks at  $2\theta = 25.3^\circ$ ,  $37.8^\circ$ ,  $48.0^\circ$ ,  $54.4^\circ$  and  $55.1^\circ$ , which corresponds to the (101), (004), (200), (105) and (211) crystal faces of anatase TiO<sub>2</sub> (JCPDS No. 21-1272), respectively. While peaks at  $2\theta = 27.4^\circ$ ,  $36.4^\circ$ , and  $41.5^\circ$ , corresponding to the (110), (101) and (111) crystal faces of rutile TiO<sub>2</sub> (JCPDS No. 21-1276), respectively [7, 11]. In addition, it can be seen in Fig. 1 that when silver is introduced into the titanium dioxide, the peaks at  $2\theta$  values of  $44.5^\circ$  can be indexed to the (200) crystalline plane of metallic silver [19, 20]. However, the peak of the graphene peak was not observed. This is because the strong diffraction peak of TiO<sub>2</sub> in  $25.3^\circ$  covers the characteristic peak of graphene, so the diffraction peak of graphene is not observed in the hydrothermally synthesized TiO<sub>2</sub>/Ag/rGO heterogeneous nanocomposites [2, 8].

### 3.2 SEM and TEM analysis

The microstructure of the sample can be observed by TEM and SEM images. Figure 2a shows the SEM images of TiO<sub>2</sub>/Ag nanowires. From Fig. 2a, we can observe that the linear structure of TiO<sub>2</sub>/Ag nanowires is obvious and size is uniform. The illustration in figure is selected area electron diffraction (SAED) pattern of TiO<sub>2</sub>/Ag/rGO nanocomposites. Its bright and round diffraction ring indicates that the TiO<sub>2</sub>/Ag/rGO nanocomposites is polycrystalline nature [21]. Figure 2b is highly magnified SEM image of TiO<sub>2</sub>/Ag/rGO nanocomposites. It can be seen from figure that the surface of the TiO<sub>2</sub>/Ag nanowire is cleaved, and a gauze-like rGO sheet is composited on the surface of the nanowire. Both the surface cracking of the nanowire and the composite of the rGO can increase the specific surface area and provide

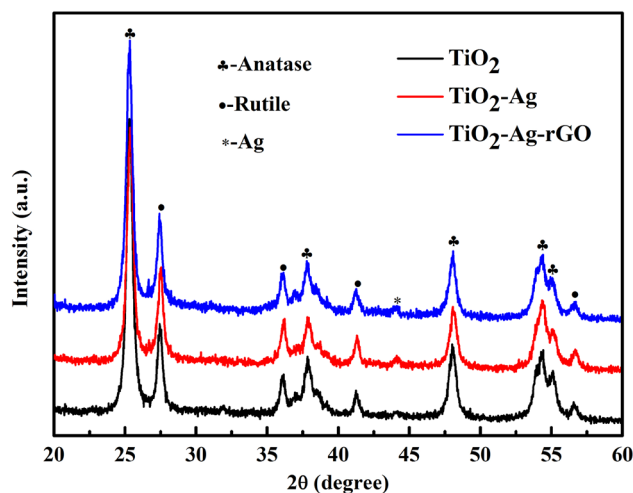


**Fig. 1** XRD patterns of TiO<sub>2</sub>, TiO<sub>2</sub>-Ag nanowires, TiO<sub>2</sub>-Ag-rGO nanocomposites

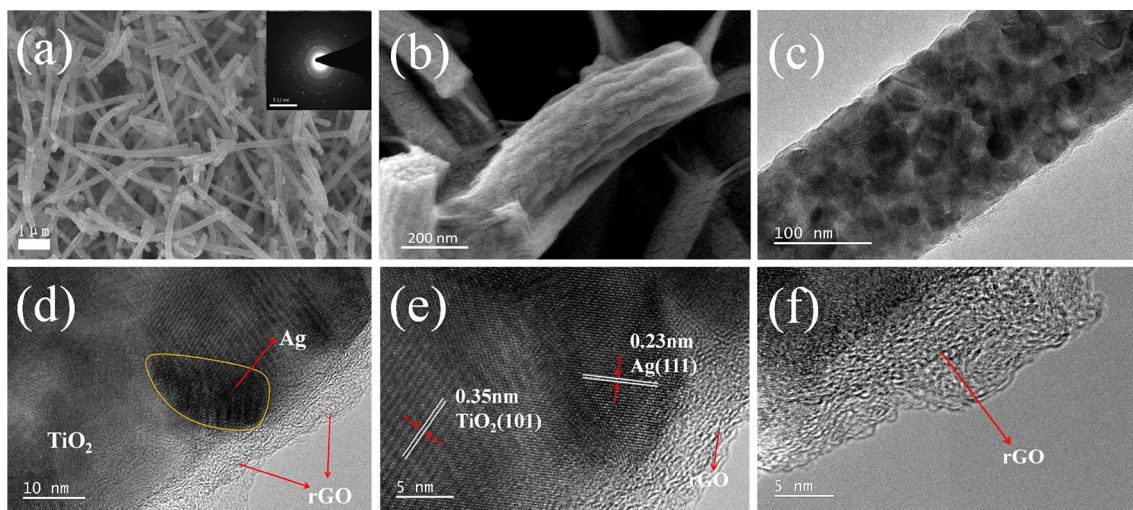


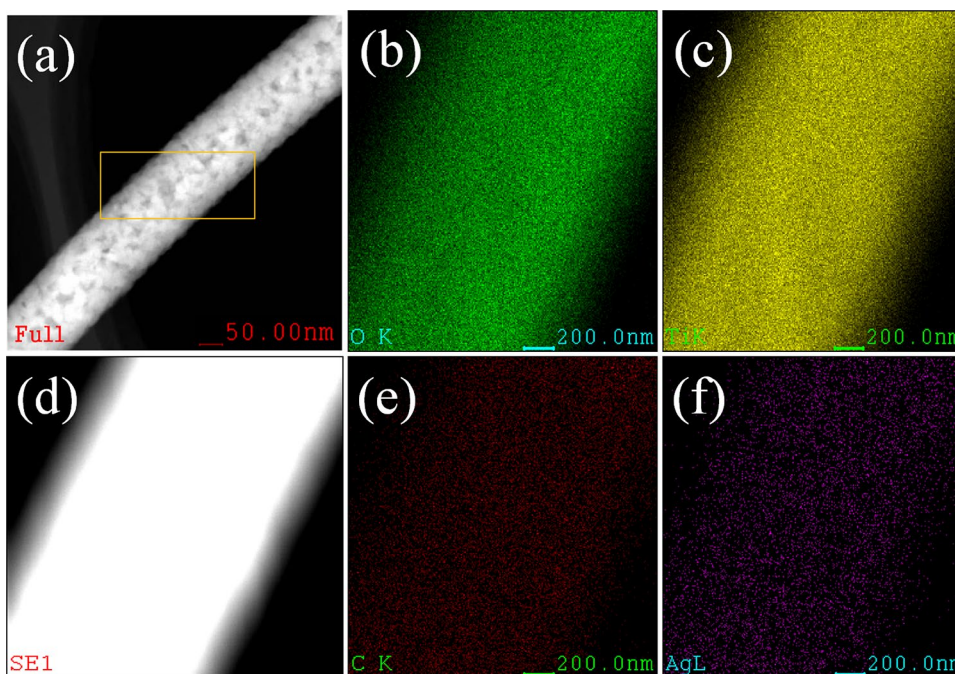
**Fig. 2** **a** is the SEM images of TiO<sub>2</sub>-Ag nanowires and the illustration is the SAED pattern of TiO<sub>2</sub>-Ag-rGO nanocomposites; **b** is the SEM images of TiO<sub>2</sub>-Ag-rGO nanocomposites; **c** is the TEM image

of TiO<sub>2</sub>-Ag-rGO nanocomposites; **d-f** are the HRTEM image of TiO<sub>2</sub>-Ag-rGO nanocomposites

more active reaction sites during photodegradation. Figure 2c is TEM images of TiO<sub>2</sub>/Ag/rGO nanocomposites. It can be observed that the results are consistent with Fig. 2b, in which rGO is tightly composited on the surface of the nanowire. Figure 2d-f are high-resolution transmission electron microscope (HRTEM) images of TiO<sub>2</sub>/Ag/rGO nanocomposites. We can see from Fig. 2d that the black part of the yellow circle that is silver, it can be further confirmed from Fig. 2e. Which the lattice fringe of the black portion can be clearly seen in Fig. 2e to be 0.23 nm, corresponding

to the (111) crystal face of Ag. In addition to this, the lattice fringes (0.35 nm) of the TiO<sub>2</sub> (101) crystal face can also be seen. Figure 2f is a HRTEM image of the rGO sheet by the edge of TiO<sub>2</sub>/Ag/rGO nanocomposites, and the characteristic image of the carbonaceous material characteristic can be clearly seen. In order to research the element distribution in the TiO<sub>2</sub>/Ag/rGO nanostructure, element mapping of O, Ti, C and Ag is performed by EDS region scanning [22, 23], as shown in Fig. 3. It can be seen from figure that the various elements are evenly distributed.

**Fig. 3** **a, d** are the HRTEM image of TiO<sub>2</sub>-Ag-rGO nanocomposites; EDS mapping images of the O (**b**), Ti (**c**), C (**e**) and Ag (**f**) elements for the TiO<sub>2</sub>-Ag-rGO nanocomposites



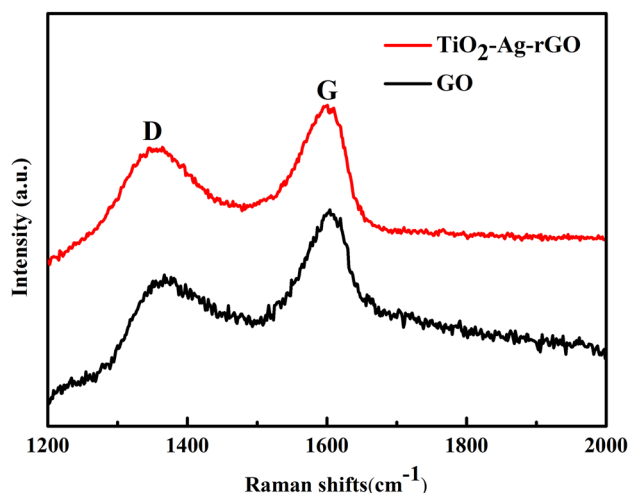


**Fig. 4** Raman spectra of GO and TiO<sub>2</sub>-Ag-rGO nanocomposites respectively

### 3.3 Raman spectra analysis

Figure 4 shows Raman spectra of GO and TiO<sub>2</sub>/Ag/rGO nanocomposites. Two obvious characteristic peaks can be seen from figure. This is a typical D-band and G-band, with a D band at 1349.3 cm<sup>-1</sup> and a G band at 1597.7 cm<sup>-1</sup>, which is exactly the same as the graphitized structure. D band and G band are attributed to disorder carbon and sp<sup>2</sup> hybridized carbon, respectively. This confirms that the high temperature and high pressure process does not destroy the components of graphene [8, 17, 24]. In addition, the intensity of the prepared I<sub>D</sub>/I<sub>G</sub> band of GO is 0.77, while the I<sub>D</sub>/I<sub>G</sub> band of TiO<sub>2</sub>/Ag/rGO nanocomposites is 0.90, which is because the oxygen functional groups in the GO are removed and reduced to the rGO. Because after hydrothermal treatment, the characteristic size of the reconstructed π-π conjugated structure in rGO is smaller than that of the original structure, resulting in an increase in I<sub>D</sub>/I<sub>G</sub> ratio [17, 25]. Therefore, an increase in the I<sub>D</sub>/I<sub>G</sub> ratio indicates that GO is successfully deoxidized during hydrothermal treatment and reduced to rGO.

### 3.4 BET analysis

A photocatalyst with a high specific surface area not only provides more reactive sites for photocatalytic reactions, but also facilitates the adsorption of target contaminants

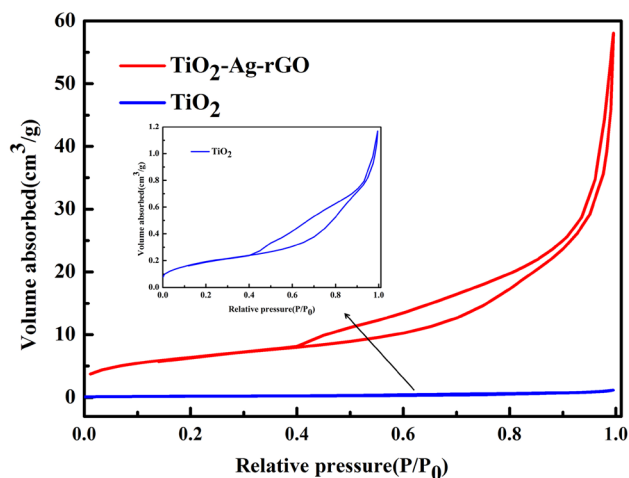


**Fig. 5** N<sub>2</sub> adsorption–desorption isotherms of TiO<sub>2</sub> nanowires and TiO<sub>2</sub>-Ag-rGO nanocomposites

by itself, thereby enhancing the catalytic efficiency of the photocatalyst [8, 24, 25]. Figure 5 is the N<sub>2</sub> adsorption–desorption curve of the prepared sample. According to international standard classification, they are classified as typical IV adsorption isotherm. From Fig. 5 the specific BET surface area of TiO<sub>2</sub>/Ag/rGO nanocomposites showed an order of magnitude change compared with TiO<sub>2</sub> nanowire. The increase in the specific surface area of TiO<sub>2</sub>/Ag/rGO nanocomposites is due to the large surface area of rGO which plays a major role in recombination.

### 3.5 XPS analysis

Figure 6a is EDX pattern of TiO<sub>2</sub>/Ag/rGO heterogeneous nanocomposites. From Fig. 6a that the chemical element composition in the prepared TiO<sub>2</sub>/Ag/rGO nanocomposites is only Ti, O, C, Ag and Cu elements, and the appearance of the Cu element is due to the EDX spectrum tested in the Cu substrate environment. In order to further analyze the composition of the material elements, the composition of the nanostructures of the TiO<sub>2</sub>/Ag/rGO heterogeneous nanocomposites and the chemical state of the elements can be tested by XPS spectroscopy. Figure 6b shows XPS spectra of TiO<sub>2</sub>/Ag/rGO heterogeneous nanocomposites only presence of Ti, C, O, Ag and without other impurity elements. Figure 7a demonstrates XPS spectra of Ti 2p, and binding energies of Ti 2p<sub>3/2</sub> and Ti 2p<sub>1/2</sub> are situated

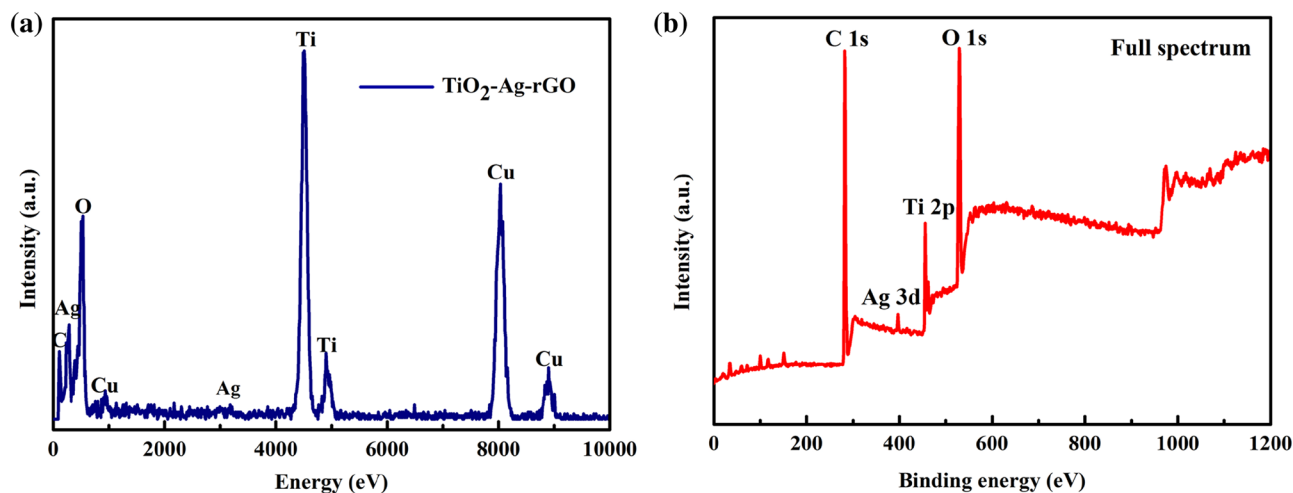


**Fig. 6** **a** is EDX and **b** is the XPS spectra wide scan spectrum of  $\text{TiO}_2\text{-Ag-rGO}$  nanocomposites

at 458.2 eV and 463.9 eV, respectively. The energy difference between  $\text{Ti } 2p_{3/2}$  and  $\text{Ti } 2p_{1/2}$  peaks is 5.7 eV, indicating that the titanium elements in the sample are all in the form of a  $\text{Ti}^{4+}$  value. Figure 7b is high-resolution XPS spectra of Ag 3d. Ag  $3d_{5/2}$  and Ag  $3d_{3/2}$  characteristic double peaks were observed at binding energies of 368.1 eV and 374.1 eV, respectively, and the separation energy between Ag  $3d_{5/2}$  and Ag  $3d_{3/2}$  was 6.0 eV. So, the XPS spectra confirm the presence of zero valent Ag in  $\text{TiO}_2/\text{Ag/rGO}$  nanocomposite [14]. Figure 7c is the higher-resolution XPS spectra of C 1s. At a binding energy of 284.6 eV, due to the C–C and C=C bonds, this indicates that the prepared rGO has a good structure. The peaks at 285.3 eV, 286.2 eV, 288.5 eV are considered to be C–OH, C–O, O–C=O, respectively [25–27]. These structures indicate that the  $\text{TiO}_2$  nanowire and the rGO in the prepared composite material are bonded by Ti–O–C bond, and are not simply physical adsorption. Such chemical bonding is advantageous for structural stability of the  $\text{TiO}_2/\text{Ag/rGO}$  heterogeneous nanocomposites.

### 3.6 UV–Vis absorption spectrum analysis

The light absorption characteristics of photocatalysts during their photodegradation are critical. Figure 8a display UV–Vis absorption spectra for sample. Seen from Fig. 8a, compared with other samples, the light absorption boundary of  $\text{TiO}_2/\text{Ag/rGO}$  nanocomposites showed a red shift. The red shift of the light absorption boundary

improves the utilization of visible light in the sample and is beneficial to increase the photocatalytic efficiency. Figure 8b shows the band widths of  $\text{TiO}_2$  nanowire,  $\text{TiO}_2/\text{Ag}$  nanowire and  $\text{TiO}_2/\text{Ag/rGO}$  nanocomposites calculated from the sample absorption spectrum and the Kubelka–Munk transformed method. As shown in Fig. 8b, the band gap of  $\text{TiO}_2$  nanowire,  $\text{TiO}_2/\text{Ag}$  nanowire and  $\text{TiO}_2/\text{Ag/rGO}$  nanocomposites are 2.93 eV, 2.88 eV and 2.83 eV respectively. Among them, the degree of narrowing of  $\text{TiO}_2/\text{Ag/rGO}$  nanocomposites is the largest, which is consistent with the analysis results of Fig. 8a. The reason for the narrowing of the band gap is caused by the impurity level introduced by the chemical bond formed between the  $\text{TiO}_2$  and the rGO, and the surface plasmon resonance effect (SPR) of silver.

### 3.7 Photocatalytic activity

The photocatalytic activity of the prepared samples was evaluated by the degree of photodegradation of the RhB solution, and the absorption peak intensity of RhB at 554 nm. Prior to photodegradation, the solution was first brought to the adsorption–desorption equilibrium, so the solution was stirred in the dark for 30 min. During the photodegradation process, the concentration of the RhB solution was measured by an UV–Vis spectrophotometer every ten minutes. A sample without any catalyst was labeled “None” to determine the self-degradation of RhB solution. Figure 9a shows the degradation curves for different

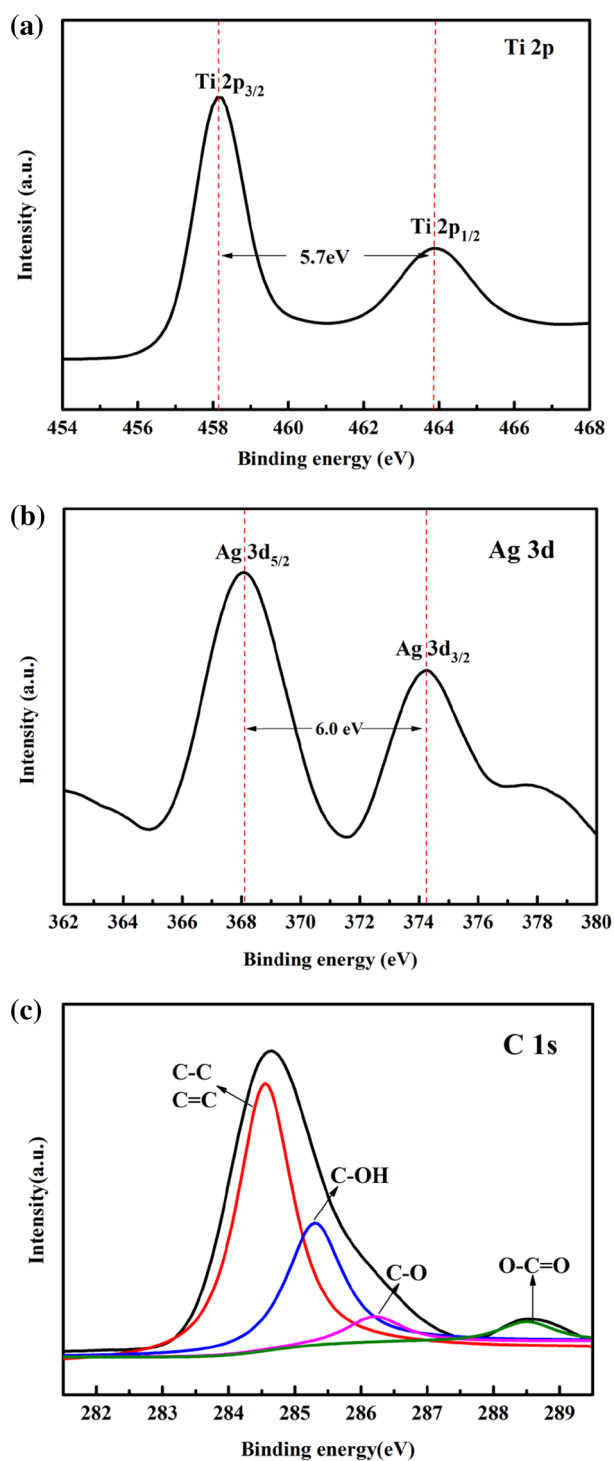


**Fig. 7** a–c is the XPS spectra high-resolution spectra of Ti 2p, Ag 3d and C 1s of TiO<sub>2</sub>-Ag-rGO nanocomposites respectively

nanocomposites, in figure  $C_0$  is the initial concentration of the RhB solution and  $C_t$  is the concentration after the xenon lamp (UV-Vis) illumination. It can be seen from Fig. 9a that only about 17% of RhB undergoes self-degradation under Xenon lamp illumination. The degradation of RhB solution in TiO<sub>2</sub> nanowire, TiO<sub>2</sub>/Ag nanowire and TiO<sub>2</sub>/Ag/rGO nanocomposites reached 76.9%, 87.7%, and 92.9%, respectively, within 80 min. Since the TiO<sub>2</sub>/Ag nanowires are combined with the rGO sheet, the specific surface area is increased, so that the adsorption capacity is obvious. At the same time, the TiO<sub>2</sub>/Ag/rGO nanocomposites showed high photodegradation activity on RhB solution, indicating that Ag and rGO sheets play an important role in enhancing the activity of photocatalyst [8, 15]. This result is more clearly and intuitively depicted in Fig. 9b. The degradation rate of all samples is shown in figure. The degradation reactions followed first-order kinetics model. The explanation was described below:  $\ln C_0/C_t = k_{app}t$ . Where,  $k_{app}$  is the apparent first-order rate constant ( $\text{min}^{-1}$ ). As can be seen in Fig. 8b, the apparent reaction rate constants ( $k_{app}$ ) for None, TiO<sub>2</sub> nanowire, TiO<sub>2</sub>/Ag nanowire and TiO<sub>2</sub>/Ag/rGO nanocomposites were  $0.00249 \text{ min}^{-1}$ ,  $0.01859 \text{ min}^{-1}$ ,  $0.02547 \text{ min}^{-1}$  and  $0.03075 \text{ min}^{-1}$ , respectively. The specific order of degradation rate was TiO<sub>2</sub>/Ag/rGO > TiO<sub>2</sub>/Ag > TiO<sub>2</sub> > None, which is in coincidence with the degradation patterns in Fig. 9a.

## 4 Conclusions

In summary, we had used a simple, efficient method for preparation of the TiO<sub>2</sub>/Ag/rGO ternary heterogeneous nanocomposites and exhibited high catalytic activity. When the Ag nanoparticles are supported of the TiO<sub>2</sub> nanowires, the Ag SPR effect increases the visible light absorption of the nanocomposites. In addition, due to the high conductivity of the rGO sheet and the metal Ag, it is advantageous for the conduction band of the TiO<sub>2</sub> to rapidly transfer electrons to prolong the lifetime of the photogenerated electron-hole pairs. Moreover, the larger specific surface area of the rGO sheet provides more active sites for photodegradation. Therefore, the noble metal and graphene and composite into a titanium dioxide semiconductor structure having a high energy band gap are promising methods for degrading pollution by using solar radiation.

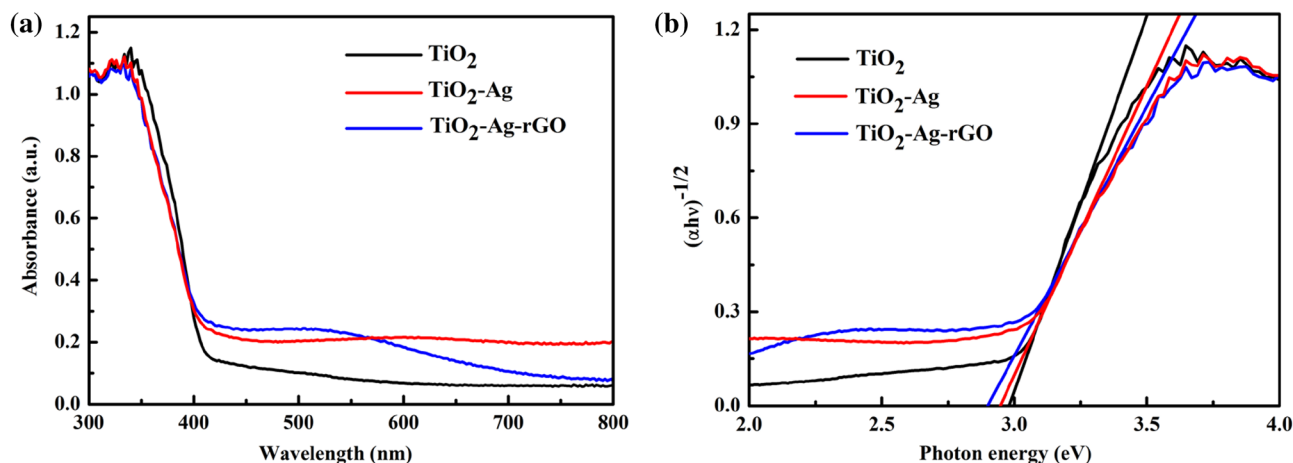


**Fig. 8** **a** UV-Vis absorption spectra and **b** plot of  $(\alpha h\nu)^{1/2}$  versus energy ( $h\nu$ ) of TiO<sub>2</sub>, TiO<sub>2</sub>-Ag nanowires, TiO<sub>2</sub>-Ag-rGO nanocomposites respectively

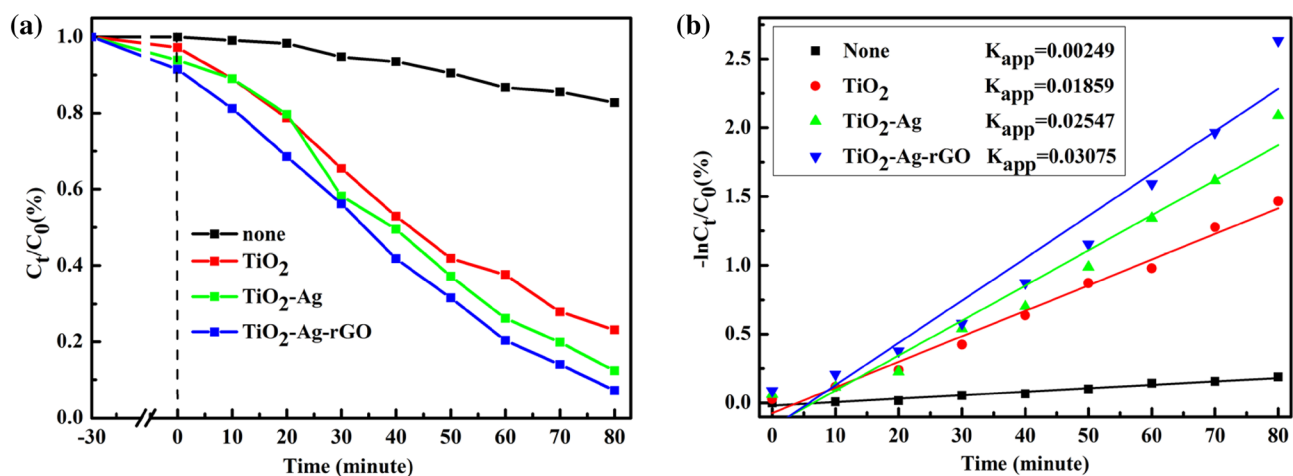


**Fig. 9** **a** Photo-degradation of RhB over different catalysts under light irradiation; **b** kinetic fitting plots of  $\ln(C_0/C_t)$  versus reaction time  $t$  for different catalysts

**Acknowledgements** This work was supported by the Fundamental Research Funds for the Higher Education Institutions of Gansu Province of China, Graduate Advisor Scientific Research Project of Gansu Province Education Department (Grant No. 1001-07), the Foundations of Northwest Normal University (Grant No. NWNLU-LKQN-10-8 and NWNLU-LKQN-09-8).

### Compliance with ethical standards

**Conflict of interest** The authors declare that there is no conflict of interest regarding the publication of this article.

### References

1. H.M. Shi, M. Zhou, D.F. Song, X.J. Pan, J.C. Fu, J.Y. Zhou, S.Y. Ma, T. Wang, *Ceram. Int.* **40**, 10383–10393 (2014)
2. Y. Choi, H. Kim, G. Moon, S. Jo, W. Choi, *ACS Catal.* **6**, 821–828 (2016)
3. B. Pant, P.S. Saud, M. Park, S.J. Park, H.Y. Kim, *J. Alloys Compd.* **671**, 51 (2016)
4. G.M. Wang, H.Q. Feng, A. Gao, Q. Hao, W.H. Jin, X. Peng, W. Li, G.S. Wu, P.K. Chu, *ACS Appl. Mater. Interfaces* **8**, 24509–24516 (2016)
5. S. Hara, M. Yoshimizu, S. Tanigawa, L. Ni, B. Ohtani, H. Irie, *J. Phys. Chem. C* **116**, 17458–17463 (2012)
6. L. Xu, X. Sun, H. Tu, Q. Jia, H. Gong, J. Guan, *Appl. Catal. B* **184**, 309–319 (2016)
7. J.X. Wei, H.M. Shi, M. Zhou, D.F. Song, Y. Zhang, X.J. Pan, J.Y. Zhou, T. Wang, *Appl. Catal. A* **499**, 101 (2015)

8. E. Vasilaki, I. Georgaki, D. Vernardou, M. Vamvakaki, N. Katsarakis, *Appl. Surf. Sci.* **353**, 865–872 (2015)
9. J.G. Wang, P.H. Rao, W. An, J.L. Xu, Y. Men, *Appl. Catal. B* **195**, 141–148 (2016)
10. Y. Zhang, T. Wang, M. Zhou, Y. Wang, Z.M. Zhang, *Ceram. Int.* **43.3**, 3118–3126 (2017)
11. N. Roy, Y. Sohn, D. Pradhan, *ACS Nano* **7**, 2532–2540 (2013)
12. H.G. Yang, C.H. Sun, S.Z. Qiao, J. Zou, G. Liu, S.C. Smith, H.M. Cheng, G.Q. Lu, *Nature* **453**, 638–641 (2008)
13. X.F. Wang, T.Y. Li, R. Yu, H.G. Yu, J.G. Yu, *J. Mater. Chem. A* **4**, 8682–8689 (2016)
14. F.Q. Gao, Y. Yang, T.H. Wang, *Chem. Eng. J.* **270**, 418 (2015)
15. M. Faraji, N. Mohaghegh, *Surf. Coat. Technol.* **288**, 144 (2016)
16. Z.M. Zhao, J. Sun, S.M. Xing, D.J. Liu, G.J. Zhang, L.J. Bai, B.L. Jiang, *J. Alloys Compd.* **679**, 88 (2016)
17. Q. Chen, M. Zhou, Z.M. Zhang, T. Tang, T. Wang, *J. Mater. Sci-Mater. Electron.* **28**, 9416–9422 (2017)
18. N. Raghavan, S. Thangavel, G. Venugopal, *Mater. Sci. Semicond. Process.* **30**, 321 (2015)
19. J. Bian, Y. Qu, R. Fazal, X. Li, N. Sun, L.Q. Jing, *J. Phys. Chem. C* **120**, 11831–11836 (2016)
20. Y. Ling, G.Z. Liao, Y.H. Xie, J. Yin, J.Y. Huang, W.H. Feng, L.S. Li, *J. Photochem. Photobiol. A* **329**, 280 (2016)
21. T. Wang, J.X. Wei, H.M. Shi, M. Zhou, Y. Zhang, Q. Chen, Z.M. Zhang, *Physica E* **86**, 103–110 (2017)
22. A. Ziarati, A. Badiei, R. Luque, W.Y. Ouyang, *J. Mater. Chem. A* **6**, 8962–8968 (2018)
23. A. Ziarati, A. Badiei, R. Luque, *Appl. Catal. B* **238**, 177–183 (2018)
24. E. Vasilaki, I. Georgaki, D. Vernardou, M. Vamvakaki, N. Katsarakis, *Appl. Surf. Sci.* **353**, 865 (2015)
25. M. Liu, R. Inde, M. Nishikawa, X. Qiu, D. Atarashi, E. Sakai, Y. Nosaka, *ACS Nano* **8**, 7229–7238 (2014)
26. O. Akhavan, M. Abdollahad, Y. Abdi, S. Mohajerzadeh, *Carbon* **47**, 3280 (2009)
27. A. Ziarati, A. Badiei, R. Luque, *Appl. Catal. B* **240**, 72–78 (2019)

**Publisher's Note** Springer Nature remains neutral with regard to jurisdictional claims in published maps and institutional affiliations.